CHEMISTRY
A EUROPEAN JOURNAL

DOI: 10.1002/chem.200601069

VIP

Structural and Magnetic Resolution of a Two-Step Full Spin-Crossover Transition in a Dinuclear Iron(II) Pyridyl-Bridged Compound

Jarrod J. M. Amoore,[a] Cameron J. Kepert,*[a] John D. Cashion,[c] Boujemaa Moubaraki,[b] Suzanne M. Neville,[b] and Keith S. Murray*[b]

Abstract: A dinuclear iron(II) complex containing the new pyridyl bridging ligand, 2,5-di(2′,2″-dipyridylamino)pyridine (ddpp) has been synthesised and characterised by single-crystal X-ray diffraction, magnetic susceptibility and Mössbauer spectral methods. This compound, $[Fe_2(ddpp)_2(NCS)_4]\cdot 4\,CH_2Cl_2$, undergoes a two-step full spin crossover. Structural analysis at each of the three plateau temperatures has revealed a dinuclear molecule with spin states HS–HS, HS–LS and LS–LS (HS: high spin, LS: low spin) for the two iron(II) centres. This is the first time that resolution of the metal centres in a HS–LS ordered state has been achieved in a two-step dinuclear iron(II) spin-crossover compound. Thermogravimetric data show that the dichloromethane solvate molecules can be removed in two distinct steps at 120 °C and 200 °C. The partially de-solvated clathrate, $[Fe_2(ddpp)_2(NCS)_4]\cdot CH_2Cl_2$, undergoes a one-step transition with an increased transition temperature with respect to the as synthesised material. Structural characterisation of this material reveals subtle changes to the coordination geometries at each of the iron(II) centres and striking changes to the local environment of the dinuclear complex. The fully de-solvated material remains high spin over all temperatures. Interestingly, the solvent can be re-introduced into the monosolvated solid to achieve complete conversion back to the original two-step crossover material, $[Fe_2(ddpp)_2(NCS)_4]\cdot 4\,CH_2Cl_2$.

Keywords: clathrates · host–guest systems · iron · magnetic properties · spin crossover

Introduction

Dinuclear spin-crossover (SCO) compounds of iron(II), iron(III) and cobalt(II) are currently receiving great interest largely because of fundamental questions concerning the synergy, if any, between the crossover transition and intramolecular exchange coupling, the latter for instance occurring between the d^6–d^6 centres in iron(II)···iron(II) compounds across covalent bridging ligands of various types and geometries.[1] The nature of the spin transition in dinuclear compounds, involving microstates HS–HS, HS–LS, LS–LS and combinations thereof (HS = high-spin; for d^6 $S = 2$, LS = low-spin; $S = 0$) is also of considerable interest, particularly from the perspective of understanding one-step versus two-step abrupt SCO transitions and how these relate to the microstates and the structures of the dinuclear molecules at particular temperatures on the spin transitions. Since the early work on bipyrimidine (bpym)-bridged iron(II) species by Kahn, Real and co-workers,[2] the subject has advanced rapidly in recent years and Real has reviewed aspects of it.[3,4] Highlights include the first one-step HS–HS to LS–LS iron(II)···iron(II) examples,[5,6] the first ordered HS–LS molecule in a "half" SCO material[7] and the first "averaged" structure of a HS–LS molecule exhibiting a two-step transition.[8] In the last case, a dicyanamide-bridged compound with pentadentate N_5-pyridyl donor "end" ligands showed structurally equivalent iron(II) centres in the plateau temperature interval between the two steps.[8]

Here we describe a new dinuclear iron(II)···iron(II) complex of formula $[Fe_2(ddpp)_2(NCS)_4]\cdot 4\,CH_2Cl_2$ (**1**·$4\,CH_2Cl_2$) that incorporates the bridging ligand (2,5-di(2′,2″-dipyridylamino)pyridine) (ddpp). The compound emanated from a wide study of different bridging ligands, such as pyrazo-

[a] J. J. M. Amoore, Prof. C. J. Kepert
School of Chemistry, University of Sydney
NSW, 2006 (Australia)
Fax: (+61) 2-9351-5741
E-mail: c.kepert@chem.usyd.edu.au

[b] Dr. B. Moubaraki, Dr. S. M. Neville, Prof. K. S. Murray
School of Chemistry, Monash University
Building 23, Clayton, Victoria, 3800 (Australia)
Fax: (+61) 3-9905-4597
E-mail: keith.murray@sci.monash.edu.au

[c] Assoc. Prof. J. D. Cashion
School of Physics, Monash University
Building 27, Clayton, VIC, Australia, 3800 (Australia)

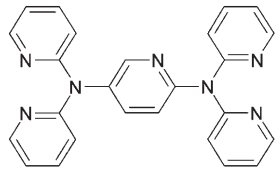

lates,[5] triazolates[9] and pyrimidine- or pyridazine-linked[10] analogues of ddpp, aimed at answering the fundamental questions posed above, when they are incorporated into dinuclear SCO iron(II) complexes. Compound **1**·4 CH_2Cl_2 is particularly relevant, because the much studied 2-step μ-bpym complexes of Real et al.[3,4] have very recently been structurally characterised at the plateau temperature and the existence of "averaged" HS–LS molecules was confirmed by noting that each iron(II) centre was structurally equivalent.[3,4] The structures of **1**·4 CH_2Cl_2 are described herein at temperatures at which the dinuclear molecules exist in the HS–HS, HS–LS and LS–LS states. In contrast to the case of $[Fe_2(NCS)_4(bt)_2(\mu\text{-bpym})]_4$,[4] the structure of the HS–LS form clearly shows an ordered HS iron(II) environment at one end and a LS iron(II) at the other end of the dinuclear moiety.

Results and Discussion

Synthesis: The ligand 2,5-di(2′,2″-dipyridylamino)pyridine (ddpp), which has not been reported previously, was synthesised by a method used for related ligands.[11]

Crystals of the dinuclear complex **1**·4 CH_2Cl_2 suitable for single crystal X-ray analysis were synthesised by slow diffusion of a solution of ddpp in dichloromethane into a solution of $Fe(ClO_4)_2$·6 H_2O and NH_4SCN in ethanol. Crystals of **1**·4 CH_2Cl_2 were partially de-solvated in vacuo, with heating to 100 °C, to yield samples of **1**·CH_2Cl_2 for magnetism and crystallographic studies. Samples of **1** were achieved by the full de-solvation of **1**·4 CH_2Cl_2 in vacuo, with heating to 200 °C.

Thermogravimetric analysis: A plot of percent mass versus temperature for a polycrystalline sample of **1**·4 CH_2Cl_2 is shown in Figure 1. Thermogravimetry clearly shows a two-step de-solvation process. The first mass loss with heating to ca. 120 °C accounts for the loss of three dichloromethane molecules (experimental: 15%, calculated 16%). The second mass loss to about 200 °C accounts for the loss of the remaining dichloromethane solvent molecule (experimental: 7%, calculated: 6.7%). The de-solvated material is stable to 350 °C, beyond which temperature it decomposes.

Magnetic properties: A plot of $\chi_M T$ versus temperature for a polycrystalline sample of **1**·4 CH_2Cl_2 is shown in Figure 2a. The SCO transition is clearly two step in character with the high-temperature step centred at 180 K, the plateau occurring between 110 K and 140 K, and the low-temperature

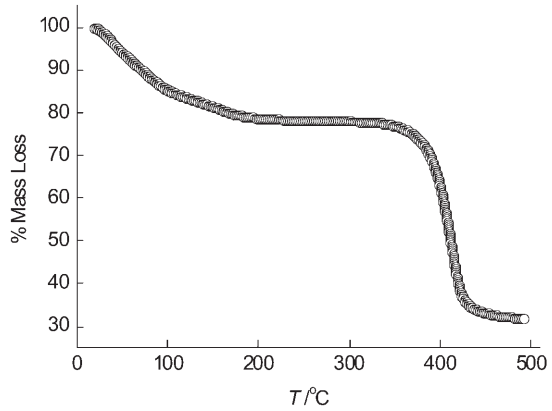

Figure 1. Thermogravimetric data for the de-solvation and subsequent thermal decomposition of **1**·4 CH_2Cl_2.

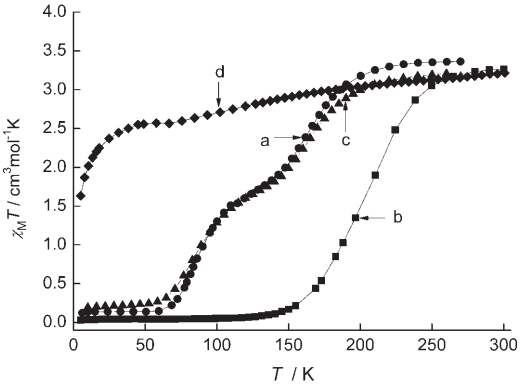

Figure 2. Plots of $\chi_M T$, per iron(II), versus temperature for complex a) **1**·4 CH_2Cl_2 (●), b) **1**·CH_2Cl_2 (■), c) re-solvated **1**·4 CH_2Cl_2 (▲) and d) **1** (◆).

step centred at 80 K. No thermal hysteresis was observed on either step. The plot is rather similar to that previously reported for a bpym-bridged iron(II) species[2–4] and that recently reported for a dinuclear dicyanamide-bridged iron(II) complex,[8] but the structural features are significantly different to those of **1**·4 CH_2Cl_2 when measured at the plateau temperature interval, as discussed below. When the sample of **1**·4 CH_2Cl_2 was partly de-solvated in vacuo under dinitrogen to remove three of the four CH_2Cl_2 molecules, a new phase, **1**·CH_2Cl_2, was obtained. The plot of $\chi_M T$ showed a single, one-step spin transition with an increased $T_{1/2}$ of 200 K, again with no thermal hysteresis (Figure 2b). Following the re-solvation of **1**·CH_2Cl_2 to give **1**·4 CH_2Cl_2 by immersion in dichloromethane, the magnetic behaviour reverted to the original two-step crossover behaviour (Figure 2c). Below 50 K, the $\chi_M T$ plot for the re-solvated **1**·4 CH_2Cl_2 sample shows a slightly higher residual magnetic moment in the LS–LS region, which is likely due to crystal cracking and deformations arising with the repeated de- and re-solvation of the crystals. Such behaviour has been reported previously.[12] When the sample of **1**·4 CH_2Cl_2 was fully de-solvated to form **1**, the resulting plot of $\chi_M T$ showed a loss of the spin transition remaining at high spin $S=2$ values, with $\chi_M T$

slowly decreasing from 3.15 $cm^3 mol^{-1} K$ at 300 K to 2.60 $cm^3 mol^{-1} K$, followed by a more rapid decrease to reach 1.6 $cm^3 mol^{-1} K$ at 4 K, the last decrease due to zero-field splitting of the $^5A_{2g}$ iron(II) states present in distorted octahedral symmetry (Figure 2d). Clearly, the spin-crossover behaviour of this dinuclear system is very sensitive to the degree of solvation.

Mössbauer spectroscopy: Mössbauer spectra measured on **1**·4 CH_2Cl_2 at 295 and 82 K are shown in Figure 3. The 295 K

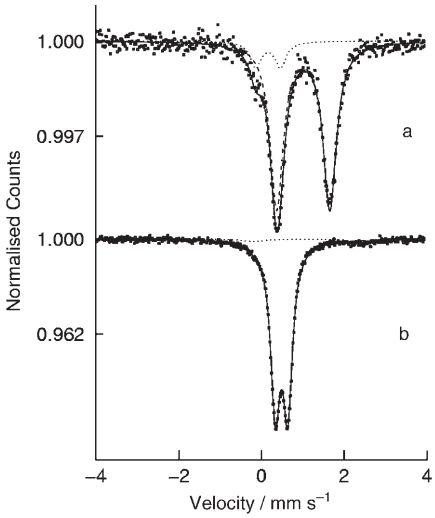

Figure 3. Mössbauer spectra of **1**·4 CH_2Cl_2 at a) 295 K and b) 82 K.

spectrum is dominated by a HS iron(II) quadrupole doublet, $\delta = 1.01$ mm s^{-1}, $\Delta E_Q = 1.29$ mm s^{-1} (88%), but has a low percentage of LS iron(II), $\delta = 0.16$ mm s^{-1}, $\Delta E_Q = 0.60$ mm s^{-1} (12%), the latter possibly originating from partial de-solvation. At 82 K, a temperature close to the middle of the second step of the spin transition, the spectrum is dominated by the LS doublet, $\delta = 0.48$ mm s^{-1}, $\Delta E_Q = 0.29$ mm s^{-1} (96.5%) with only a small HS doublet evident, $\delta = 1.08$ mm s^{-1}, $\Delta E_Q = 2.5$ mm s^{-1} (3.5%). The value of $\chi_M T$ at 82 K (Figure 2) would suggest that approximately 20% HS iron(II) should be present. Even allowing for Debye–Waller changes, this again suggests that partial loss of CH_2Cl_2 has occurred in the sample used for Mössbauer spectroscopy. The isomer shifts and quadrupole splitting values observed are typical of such *cis*-Fe$(NCS)_2(N)_4$ coordination environments, as are their variations with temperature.

X-ray crystallography

The structure of ***1*·4 CH_2Cl_2***: The asymmetric unit of **1**·4 CH_2Cl_2 contains one complete dinuclear unit with two crystallographically distinct iron(II) centres, four thiocyanate ligands, two ddpp ligands and four dichloromethane solvent molecules (Figure 4). The two ddpp ligands in each dinuclear unit bridge the iron(II) centres and are arranged in a "head-to-tail" fashion. Each ddpp ligand binds through two

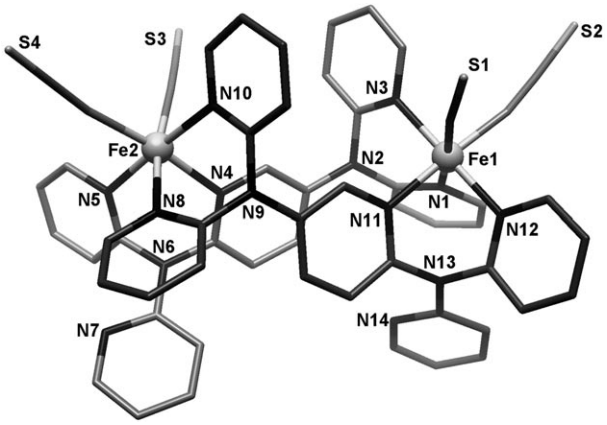

Figure 4. The structure of the dinuclear complex $[Fe_2(ddpp)_2(NCS)_4]$ of **1**·4 CH_2Cl_2 at 250 K. The solvent molecules and hydrogen atoms have been omitted for clarity.

different bidentate chelation modes: the first consists of a typical di(2-pyridyl)amine-style coordination through the two terminal pyridine rings, and the second mode involves the central pyridine ring nitrogen atom and one terminal di(2-pyridyl)amine pyridyl ring. Conformationally, the dinuclear complex has near-C_2 symmetry, the most notable deviation from this being at the periphery of the molecule: the uncoordinated pyridine ring closest to Fe1 points back towards the centre of that ligand, while that closest to Fe2 is rotated such that it faces away from the centre of the ligand (Figure 4).

Full structural analysis of **1**·4 CH_2Cl_2 was carried out at three temperatures, 250, 123 and 25 K, a range that encompasses the full two-step spin transition, and revealed a dinuclear material with iron(II) centres in the HS–HS, HS–LS and LS–LS states, respectively. A summary of the crystal data and refinement results is given in Table 1. The dinuclear unit contains two structurally inequivalent iron(II) centres, Fe1 and Fe2, at each temperature. Table 2 summarises the Fe–N bond lengths of each iron(II) centre over the three temperatures measured. At 25 K, both the Fe atoms in **1**·4 CH_2Cl_2 are in the LS state with Fe–N bond lengths between 1.933(3)–1.998(3) Å for Fe1 and 1.958(3)–2.016(3) Å for Fe2. At 250 K, both Fe atoms are in the HS state with Fe–N bond lengths between 2.089(4)–2.236(3) Å for Fe1 and 2.105(3)–2.234(3) Å for Fe2. At 123 K, the Fe–N bond lengths are consistent with a HS–LS intermediate in which the HS and LS states are localised on the structurally inequivalent iron(II) sites: Fe1 is in the LS state, with Fe–N bond lengths in the range 1.950(2)–2.010(2) Å and Fe2 is in the HS state with bond lengths in the range 2.064(3)–2.197(2) Å. The minor decreases in bond length for Fe1 (LS) on cooling from 123 to 25 K and for Fe2 (HS) on cooling from 220 to 123 K are consistent with thermal bond contraction associated with decreased thermal population of the Fe–N stretching vibrations, although these may also reflect a small degree of partial HS/LS at these sites. This is the first time crystallographic resolution of an intermediate HS–LS state has been achieved in a dinuclear material that un-

Table 1. Single-crystal diffraction data and refinement parameters for **1**·4 CH_2Cl_2 and **1**·CH_2Cl_2.

	1·4 CH_2Cl_2	**1**·4 CH_2Cl_2	**1**·4 CH_2Cl_2	**1**·CH_2Cl_2
spin states	LS–LS	HS–LS	HS–HS	HS–HS
formula	$Fe_2S_4C_{58}H_{42}N_{18}Cl_8$	$Fe_2S_4C_{58}H_{42}N_{18}Cl_8$	$Fe_2S_4C_{58}H_{42}N_{18}Cl_8$	$Fe_2S_4C_{55}H_{36}N_{18}Cl_2$
M_r [g mol^{-1}]	1518.67	1518.67	1518.67	1263.89
T [K]	25(2)	123(2)	250(2)	250(2)
crystal system	triclinic	triclinic	triclinic	triclinic
space group	$P\bar{1}$	$P\bar{1}$	$P\bar{1}$	$P\bar{1}$
Z	2	2	2	2
a [Å]	14.050(4)	14.1979(9)	14.356(11)	13.9416(9)
b [Å]	14.100(4)	14.2112(9)	14.565(12)	14.3783(9)
c [Å]	17.906(6)	17.8925(11)	17.986(14)	17.6480(11)
α [°]	79.001(5)	78.7370(10)	79.546(13)	78.748(2)
β [°]	77.807(5)	79.6240(10)	79.770(13)	77.073(4)
γ [°]	66.817(4)	67.2180(10)	66.840(12)	63.497(3)
V [Å^3]	3164.5(17)	3242.5(4)	3377(5)	3067(2)
ρ_{calcd} [mg m^{-3}]	1.594	1.555	1.494	1.369
μ [mm^{-1}]	0.985	0.961	0.923	0.748
data/restraints/parameters	13244/0/811	14738/0/811	15229/0/811	18842/0/724
$R(F)$ [%] ([$I>2\sigma(I)$], all)	4.45(5.22)	5.07(6.03)	6.07(8.31)	14.00(19.41)
$R_w(F^2)$ [%] ([$I>2\sigma(I)$], all)	12.22(13.11)	13.47(14.47)	16.65(19.17)	28.05(30.45)
GoF	1.063	1.037	1.034	1.313

Table 2. Selected bond lengths [Å] of the complex **1**·4 CH_2Cl_2 in the LS–LS (25 K), HS–LS (123 K) and HS–HS (250 K) states, and **1**·CH_2Cl_2 in the HS–HS (123 K) state.

	1·4 CH_2Cl_2			**1**·CH_2Cl_2
	LS–LS	HS–LS	HS–HS	HS–HS
Fe1–N1	1.978(2)	1.995(2)	2.216(3)	2.217(6)
Fe1–N3	1.991(3)	2.009(2)	2.236(3)	2.202(6)
Fe1–N11	1.985(2)	1.997(2)	2.203(3)	2.215(5)
Fe1–N12	1.998(3)	2.010(2)	2.215(3)	2.208(5)
Fe1–N15	1.950(3)	1.951(2)	2.097(4)	2.113(7)
Fe1–N16	1.933(3)	1.950(2)	2.089(4)	2.126(8)
Fe2–N4	2.013(2)	2.197(2)	2.225(3)	2.215(6)
Fe2–N5	1.994(3)	2.179(3)	2.215(4)	2.202(7)
Fe2–N8	2.004(3)	2.178(2)	2.234(3)	2.201(5)
Fe2–N10	2.016(3)	2.192(2)	2.229(4)	2.217(6)
Fe2–N17	1.962(3)	2.103(3)	2.115(4)	2.120(7)
Fe2–N18	1.958(3)	2.064(3)	2.105(3)	2.056(7)

dergoes a full HS–HS to LS–LS transition. We note that an ordered HS–LS state has been observed in a triazole bridged compound,[7] but here the LS–LS state was not reached at temperatures below $T_{1/2}$. In the case of a two-step pyrazolate-bridged iron(II) compound, the structure obtained at the plateau region of a two-step transition showed a 50:50 occurrence of dinuclear molecules in the HS–HS and LS–LS states.[12]

The two crystallographically distinct iron(II) atoms in each dinuclear moiety are in a distorted octahedral geometry consisting of two NCS^- ions in a *cis* arrangement and four pyridine rings from two separate ddpp ligands. While the coordination environments of the two crystallographically distinct iron(II) sites are very similar due to the near-C_2 symmetry of the complex, subtle differences in their geometry exist. These differences have been quantified by using the octahedral distortion parameter, Σ,[14] a measure of the angular deviation from octahedral geometry, in Table 3. Recent comparative studies have shown that minimal Σ values are associated with stronger crystal fields and, therefore, to the stabilisation of the low-spin state.[15] Here, a strong correlation is found between the octahedral distortion and the occurrence of spin crossover at each of the metal sites. For **1**·4 CH_2Cl_2 at 250 K, in which both the iron(II) centres are in the high-spin state, the Σ parameters for Fe1 and Fe2 are 41.8 and 46.7°, respectively, indicating that Fe1 has the more regular geometry; this is consistent with the observation that Fe1 is the first to convert to LS upon cooling. At 25 K, in which both iron(II) centres are in the low-spin state, more regular octahedral geometries are observed, with $\Sigma = 28.4°$ for Fe1 and 35.2° for Fe2. In the intermediate HS–LS state at 123 K, $\Sigma = 27.7°$ for Fe1 (LS) and 45.9° for Fe2 (HS). Interestingly, it would appear that the spin crossover at the Fe1 site with cooling from 220 to 123 K does little to influence the geometry of the Fe2 site, there being only a small change in Σ of Fe2 from 46.7 to 45.9°. This is further highlighted in the relatively small change to the individual Fe–N distances and angles (maximum distance and angle deviations; Fe2–N8: 0.056 Å and N8-Fe2-N10: 1.36°). Similarly, spin crossover at the Fe2 with cooling from 123 to 25 K has little influence on the geometry of the low spin Fe1 site, its Σ parameter changing from 27.7 to 28.4° and the individual distance and angles also being similar (maximum distance and angle deviations; Fe1–N3: 0.018 Å and N15-Fe1-N1: 0.45°). These combined observations suggest there is little in the way of steric coupling between the two crossover centres, and that the dinuclear complex is sufficiently flexible to accommodate geometry changes at one metal site, whilst retaining what would appear to be a locally optimal coordination geometry at the other. It seems likely also that there will be only relatively minor electronic coupling between the two metal sites through the six-atom bridge of the ddpp ligand. As such, it is difficult to determine the degree and nature of any synergy between these sites in favouring or disfavouring spin crossover at the other.

A number of intra- and intermolecular π–π stacking interactions exist in **1**·4 CH_2Cl_2. Within the dinuclear complex, π–π stacking is seen between the two central pyridyl rings on each ligand, a (Figure 5 left, Table 3), and between the unbound pyridyl donor groups, b (Figure 5 right, Table 3). The dinuclear molecules are arranged in chains along the [111] direction of the unit cell. Two rather long π–π stacking interactions are observed between pyridyl rings belonging to adjacent chains (centroid-to-centroid distances 4.01 and 4.14 Å) (Figure 6). Such effects have been thought to be important in spin transitions in μ-bpym compounds, such as

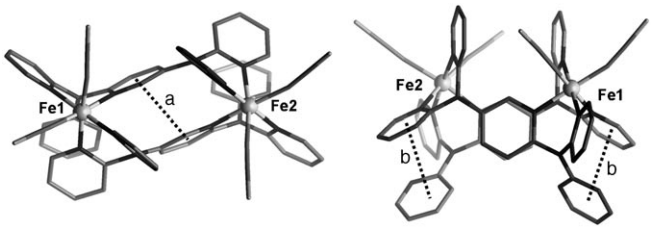

Figure 5. Two types of π–π stacking interactions within the dinuclear **1**·4 CH_2Cl_2 between central pyridyl rings, a (left), and between uncoordinated pyridyl rings and di(2-pyridyl)amine rings, b (right).

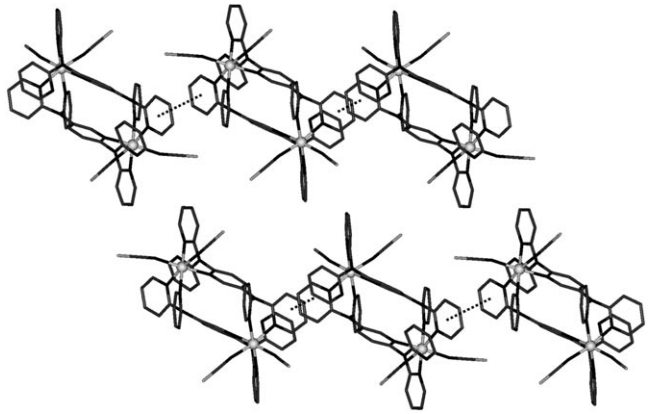

Figure 6. Crystal packing of the dinuclear molecules in **1**·4 CH_2Cl_2.

$[Fe_2(\mu\text{-bpym})(NCS)_4(bt)_2]$, in which bt is *bis*-thiazoline.[2–4] In addition, there are multiple interactions between dinuclear complexes and between dinuclear and solvent molecules; these involve all four sulfur atoms from the thiocyanate ligands and three of the four solvent molecules (Figure 7, top). There are three types of sulfur interactions

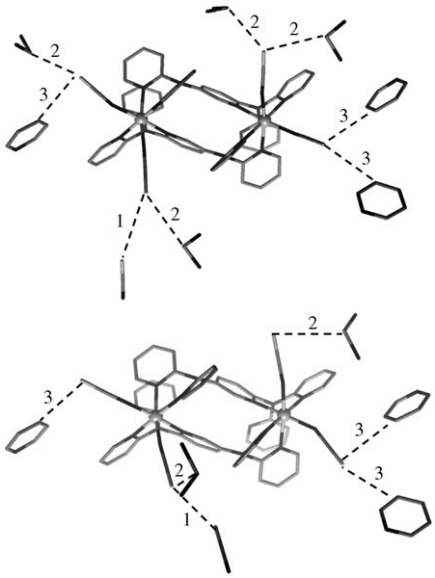

Figure 7. Comparison of the three types of short contacts in the local environments of **1**·4 CH_2Cl_2 (top) and **1**·CH_2Cl_2 (bottom). 1: S···S, 2: S···C-(H_2Cl_2), 3: S···C(H_3C_3N). Hydrogen atoms have been omitted for clarity.

(Figure 7 top, Table 3): the first are S···S interactions to adjacent dinuclear complexes (Table 3, 1; S4···S2); the second are S···HC interactions to solvent dichloromethane molecules (Table 3, 2; S2···C56, S2···C55, S3···C57, S4···C58) and the third are S···HC interactions to aromatic rings on adjacent dinuclear molecules (Table 3, 3; S1···C21, S1···C43). All these interactions contract in distance with cooling, with the exception of S3···C57, which expands (Table 3).

Variable-temperature unit-cell analysis on ***1·4 CH_2Cl_2***: In addition to full structural characterisations in each of the spin

Table 3. Comparison of bond lengths and angles of the complex **1**·4 CH_2Cl_2 in the LS–LS (25 K), HS–LS (123 K) and HS–HS (250 K) states, and **1**·4 CH_2Cl_2 in the HS–HS state.

	1·4 CH_2Cl_2			**1**·CH_2Cl_2
spin state	LS–LS	HS–LS	HS–HS	HS–HS
T [K]	25(2)	123(2)	250(2)	250(2)
M···M distance [Å]	7.0654(15)	7.1585(6)	7.324(4)	7.298(13)
$\langle d_{Fe1-N}\rangle$ [Å]	1.972(3)	1.985(3)	2.176(3)	2.168(5)
$\langle d_{Fe2-N}\rangle$ [Å]	1.991(2)	2.152(3)	2.187(4)	2.181(5)
N-Fe1-N range [°]	86.45–96.11	86.21–95.78	80.81–97.83	82.10–95.60
N-Fe2-N range [°]	86.43–96.04	82.16–96.97	80.97–96.65	81.90–95.70
Σ_{Fe1} [°][a]	28.4	27.7	41.8	42.4
Σ_{Fe2} [°][a]	35.2	45.9	46.7	40.4
intramolecular π–π stacking a [Å][b]	3.395(2)	3.4584(15)	3.581(4)	3.695(4)
intramolecular π–π stacking b [Å][b]	3.5765(19), 3.841(2)	3.6010(17), 3.880(2)	3.680(4), 3.867(4)	3.608(5), 3.791(5)
intermolecular π–π stacking [Å]	4.045(2), 4.027(2)	4.0595(16), 3.9757(18)	4.132(4), 4.043(4)	3.594(5), 3.785(4)
S···S interaction [Å], 1[c]	3.624(2)	3.843(2)	4.216(5)	3.352(6)
S···C(H_2Cl_2) interaction [Å], 2[c]	3.441(3), 3.545(3), 3.742(3), 3.552(3), 3.590(3)	3.506(5), 3.636(4), 3.698(4), 3.607(4), 3.636(4)	3.551(12), 3.686(10), 3.617(8), 3.672(8), 3.797(7)	3.928(20), 3.768(20)
S···C(H_4C_4N) interaction [Å], 3[c]	3.515(3), 3.688(3)	3.512(3), 3.745(3)	3.594(5), 3.737(5)	3.481(9), 3.816(9)

[a] Σ = sum of the deviation of each of the 12 *cis* angles from 90°.[14,15] [b] π–π stacking a and b; see text and Figure 5 for definitions. [c] Short contacts 1, 2 and 3; see text and Figure 7 for definitions.

states, the spin transition in **1**·4 CH_2Cl_2 was followed by in-situ, single-crystal, variable-temperature, unit-cell data collections between 25 to 250 K. Figure 8 shows the percentage of unit-cell variation over the transition for each unit-cell

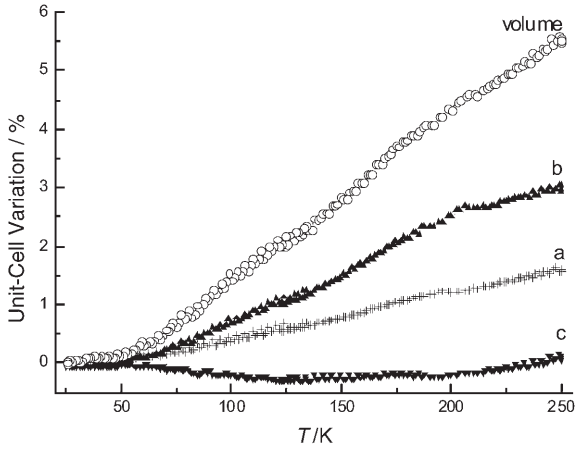

Figure 8. Percentage variation in the unit-cell volume (○) and the *a* (+), *b* (▲) and *c* axes (▼) for complex **1**·4 CH_2Cl_2 determined by single-crystal X-ray diffraction.

axis and for the unit-cell volume. The overall change in unit-cell volume shows an approximately linear decrease between 250 and 55 K, followed by a plateau down to 25 K. The *a* and *b* axes show similar decreases to those seen in the unit-cell volume, from 250 to 25 K, as is expected from the contraction in Fe–N bond lengths associated with the spin transition. In contrast, the *c* axis is seen to increase in length as the temperature decreases from 150 to 55 K. This correlates to an observed expansion in the ligand central ring π–π stacking distance from the HS to LS states. The overall rate of decrease in the unit-cell volume matches the magnetic susceptibility plot, which reaches the LS–LS values at approximately 55 K after a gradual two-step decrease from 250 K (Figure 2a).

The two-step character of the transition is evident as a number of subtle features in Figure 8, but is not as defined as in the magnetic susceptibility data. The HS–HS plateau in Figure 2 occurs at 190–200 K and correlates with maximum values in the *a*, *b*, and *c* axes and volume at 190, 205, 185 and 205 K, respectively. The HS–LS plateau in Figure 2 occurs at 120–130 K and correlates with maximum values in the *a* and *b* axes and volume at 130 K and minimum values in the *c* axis at 130 K. The LS–LS plateau in Figure 2 occurs below 60 K and corresponds with a plateau in the *a*, *b* and *c* axes and volume below 55 K. While there are numerous examples of variable-temperature, unit-cell data for mononuclear systems, no such multi-temperature unit-cell data of other two-step (or one-step), spin-crossover dinuclear iron(II) species are available for comparison. Multiple-temperature structural analysis was reported recently by Real et al.[8] for a dicyanamide-bridged iron(II) compound and it revealed a correlation between average Fe–N bond length, over the dinuclear moiety, and magnetic susceptibility, including the two-step plateau. This is not appropriate here as a distinct intermediate HS–LS state has been confirmed both magnetically and structurally rather than the nonordered example above.

The structure of ***1***·CH_2Cl_2: As indicated above, thermogravimetric analysis on **1**·4 CH_2Cl_2 revealed a two-step de-solvation process over the temperature range 25–200 °C. Structural analysis of the partially de-solvated material was carried out by heating a single crystal, in situ, at 20 $K\,h^{-1}$ from room temperature to 375 K. Remarkably, the crystals remained single following guest desorption (Figure 9). Structural analysis was carried out at 250(2) K, revealing the partially solvated analogue, $[Fe_2(ddpp)_2(NCS)_4]$·CH_2Cl_2 (**1**·CH_2Cl_2). The conformation of the dinuclear complex remains essentially unchanged following solvent desorption, with the unit retaining its near-C_2 local symmetry with two crystallographically distinct iron(II) centres. As in **1**·4 CH_2Cl_2, the most notable deviation from a C_2 configuration is the alignment of the unbound pyridyl units of the ddpp ligand. The single CH_2Cl_2 guest retained in this structure is disordered over two crystallographically distinct sites (occupancy ratio 78:22 %).

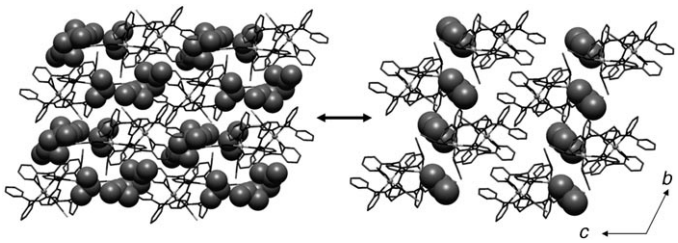

Figure 9. In situ single crystal-to-crystal transformation from **1**·4 CH_2Cl_2 (left) to **1**·CH_2Cl_2 (right) viewed along the *a* axis; atoms of the dinuclear complex are represented as sticks and of the CH_2Cl_2 as balls. The minor component of CH_2Cl_2 disorder in **1**·CH_2Cl_2 is omitted for clarity.

The Fe–N distances for both iron(II) centres of **1**·CH_2Cl_2 at 250 K are consistent with high-spin iron(II), as expected from magnetic susceptibility data for which this is close to the onset of the HS–HS plateau of the spin transition (Figure 2, Table 1). There are only very slight differences in their environments in this case with $\Sigma = 42.4$ and 40.4° for Fe1 and Fe2, respectively (Table 3). Perhaps unexpectedly, de-solvation of **1**·4 CH_2Cl_2 to form **1**·CH_2Cl_2 yields a dinuclear complex with an enhanced crystal field at each site, as evidenced by the increase in spin-crossover transition temperature for this phase and the retention of moderate values of Σ. In contrast, we have shown that de-solvation of the nanoporous spin-crossover framework material $[Fe(azpy)_2(NCS)_2]$·*x*(guest) (azpy = 4,4′-azopyridine)[16] destabilises the low-spin state due to adoption of relatively unfavourable iron(II) geometries in the apohost. Similarly, Real et al. have shown that removal of both bound and unbound water in $[Fe^{II}(pmd)(OH_2)\{M^{I}(CN)_2\}_2]$·$H_2O$ (pmd = pyrimidine; M = Ag, Au) destabilises the low-spin state.[17] Dehydration

of the SCO Hofmann clathrate phase $[Fe^{II}(pz)\{Pt^{II}(CN)_4\}]\cdot n(H_2O)$ (pz = pyrazine; $n \approx 2$–3), however, leads to an increase in the spin-crossover temperature.[18]

Whereas a significant difference exists in the octahedral distortion between the Fe1 and Fe2 centres in **1**·4 CH_2Cl_2, in **1**·CH_2Cl_2 there is relatively little difference between these geometries. This is consistent with the observed change from two-step to apparent one-step character. The overlaying in temperature of the two spin-crossover transitions, one for each of the crystallographically distinct, but very similar, iron(II) environments, to give an apparent single-step transition supports the view that there is little in the way of intramolecular coupling between the metal centres in this complex, and that crystal packing is the dominant influence in determining the crossover properties. This is in contrast to that observed, for example, in the 2×2 grid complex, $[Fe_4(L)_4(ClO_4)_8]$ (L = 4,6-bis(2′,2″-bipyrid-6′-yl)-2-phenylpyrimidine),[19] in which crossover occurring at the inequivalent iron(II) sites seems to have an antagonistic effect against spin crossover at the other three sites.

As with **1**·4 CH_2Cl_2, both inter- and intramolecular π–π stacking interactions exist in **1**·CH_2Cl_2, all of these being shortened following solvent desorption (Table 3). This contraction is highlighted by a reduction in the crystal volume occupied by solvent and void, which totals 27.1% (25.9% solvent, 1.2% void) for **1**·4 CH_2Cl_2 and 20.2% (11.3% solvent, 8.7%, void) for **1**·CH_2Cl_2.[20] There are multiple contacts between adjacent dinuclear complexes and between dinuclear complexes and the solvent molecule, as observed in **1**·4 CH_2Cl_2. Three types of sulfur interactions are present in **1**·CH_2Cl_2 (Figure 7 bottom, Table 3), which include all four sulfur atoms and the one remaining solvent molecule. Firstly, S···S interactions are present (Table 3, 1; S4···S4), but here they are between symmetry equivalent atoms on the neighbouring dinuclear, that is, between sulfur atoms connected to Fe1, whereas in **1**·4 CH_2Cl_2 they are between sulfur atoms connected to Fe1 and Fe2; secondly, S···C(H_2Cl_2) interactions are present between the dinuclear and solvent molecule (Table 3, 2; S2···C55, S4···C55), but there are fewer interactions due to the decrease in number of solvent molecules; and thirdly, there are S···C(H_4C_4N) interactions to adjacent dinuclear molecules (Table 3; 3; S1···C21, S3···C29). We attribute the stability of the monosolvate in a narrow temperature range to the stabilising influence of the interactions to the one remaining solvent per dinuclear unit.

Conclusions

Compound **1**·4 CH_2Cl_2 has provided important new structural data on the nature of the spin transition in dinuclear iron(II) spin-crossover materials, particularly in regard to two-step transitions for which it provides the first structure of the HS–LS molecules at the plateau region. The small differences noted in coordination geometries of Fe1 and Fe2, at all temperatures studied, suggest that these play a part in the two-step mechanism. The loss of the step when **1**·4 CH_2Cl_2 is partially de-solvated to form **1**·CH_2Cl_2, and the loss of the spin transition when **1**·4 CH_2Cl_2 is fully de-solvated to form **1**, suggest that interdimer crystal packing effects play a key role in influencing the crossover properties. In their recent article on the bpym-bridged iron(II) family, as well as summarising the uses of applied field Mössbauer spectroscopy and the LIESST effect in probing the mechanism of 2-step transitions, Real and co-workers[4] point out that interdimer interactions in the solid state play a delicate balancing role with the intramolecular interactions in stabilising HS–LS states. From this perspective, we have recently crystallised other solvates of **1** and are investigating their properties.

In surveying the advances made in the last two years in terms of intradinuclear bridging ligands and bridging geometry/rigidity, it is tempting to speculate that the flexible nature of the bridging in **1**·4 CH_2Cl_2 provides less rigid environments around the iron(II) centre than in the di-μ-pyrazolate,[5,6,12] di-μ-triazole[7] or μ-bpym[2–4] systems, thus allowing stabilisation of dinuclear molecules in the HS–HS, HS–LS and LS–LS states. Structural nuances of these kinds are difficult to assess in their importance compared to the electronic HS→LS driving forces/energies. The influence of antiferromagnetic exchange across the various bridges on the spin-transition mechanism is even more difficult to assess, since it is generally very weak in magnitude, the J values being about $-4\ cm^{-1}$ for the bpym bridge down to about zero in **1**·4 CH_2Cl_2. Zein and Borshch have discussed these effects, recently, in density functional theory calculations of the HS–HS, HS–LS and LS–LS energies in dinuclear iron(II) SCO compounds.[21]

We are presently pursuing LIESST studies on **1**·4 CH_2Cl_2 and **1**·CH_2Cl_2 and are synthesising other bridging groups of the ddpp type, but containing pyrimidine and pyridazine linkers between dipyridylamine and dipyridylmethane chelators that will lead to different bridging geometries being formed between iron(II) centres.

Experimental Section

Synthesis of ddpp: All chemicals were obtained from Aldrich and Fluka and used without further purification. A solution of 2,2′-dipyridylamine (10.71 g, 62.9 mmol) in dichloromethane (20 mL) was added to a stirred solution of 2,5-dibromopyridine (4.68 g, 19.7 mmol) in dichloromethane (20 mL). Aqueous solutions of anhydrous potassium carbonate (9.34 g in 20 mL; 67.6 mmol) and copper sulfate pentahydrate (1.42 g in 10 mL; 5.69 mmol) were then added and the mixture stirred vigorously for 10 min before being evaporated to dryness under vacuum. The mixture was then ground thoroughly with a mortar and pestle; a small amount of dichloromethane (2 mL) was added and the mixture heated to 483 K for 21 h under a dinitrogen atmosphere. The mixture was dissolved in chloroform (100 mL) and water (200 mL). The water layer was washed with chloroform (50 mL) and the organic layers combined and washed with water (5×100 mL). The organic portion was reduced in volume to give a light yellow-brown powder. This powder was recrystallised using ethanol to give a cream coloured powder (3.21 g, 39%). ^{1}H NMR (300 MHz, [D]chloroform): $\delta = 8.39$ (ddd, $J = 4.79$, 1.81, 0.59 Hz, 2H), 8.32 (ddd, $J =$ 4.81, 1.80, 0.62 Hz, 2H), 8.18 (dd, $J = 2.91$, 0.55 Hz, 1H), 7.62 (m, $J = 7.35$, 2.07 Hz, 4H), 7.49 (dd, $J = 8.72$, 2.81 Hz, 1H), 7.15 (dd, $J = 7.43$, 0.93 Hz,

2H), 7.11 (d, $J=0.53$ Hz, 1H), 7.07 (ddd, $J=8.10$, 1.64, 0.91 Hz, 2H), 7.03 (ddd, $J=7.37$, 5.09, 1.03 Hz, 2H), 6.96 ppm (ddd, $J=7.27$, 5.09, 0.96 Hz, 2H); ^{13}C NMR (300 MHz, [D]chloroform): $\delta=157.7$ (2C, py), 157.4 (2C, py), 154.1 (1C, py), 149.0 (2C, py), 148.7 (2C, py), 147.2 (1C, py), 138.0 (4C, py), 137.3 (1C, py), 136.3 (1C, py), 119.6 (2C, py), 119.1 (2C, py), 118.8 (2C, py), 118.7 (1C, py), 117.0 ppm (2C, py); ESI-HRMS (positive ion mode, dichloromethane/methanol): m/z calcd for $C_{25}H_{19}N_7$+Na: 440.15969; found: 440.15968; error: 8×10^{-6}.

Synthesis of $[Fe_2(ddpp)_2(NCS)_4]\cdot4CH_2Cl_2$ ($\mathbf{1}\cdot4CH_2Cl_2$): Complex $\mathbf{1}\cdot4CH_2Cl_2$ was synthesised by the slow diffusion of a solution of ddpp (23.1 mg, 5.53×10^{-5} mol) in dichloromethane (5 mL) into a solution of iron(II) perchlorate hexahydrate (19.4 mg, 5.35×10^{-5} mol) and ammonium thiocyanate (11.4 mg, 1.52×10^{-4} mol) ethanol (3 mL). Light yellow rectangular rod shaped crystals suitable for X-ray diffraction and magnetic susceptibility measurements were produced.

Synthesis of $[Fe_2(ddpp)_2(NCS)_4]\cdot CH_2Cl_2$ ($\mathbf{1}\cdot CH_2Cl_2$): Complex $\mathbf{1}\cdot CH_2Cl_2$ was converted directly from $\mathbf{1}\cdot4CH_2Cl_2$ in vacuo with heating to 100°C under dry dinitrogen. For structural analysis, a single crystal of $\mathbf{1}\cdot4CH_2Cl_2$ was heated under a dinitrogen stream at 20 K h^{-1} from room temperature to 375 K, allowed to stand at 375 K for 4 h, and subsequently cooled to 250 K for data collection.

Crystallographic data collection and refinement: Diffraction data for $\mathbf{1}\cdot4CH_2Cl_2$ at 25(2), 123(2) and 250(2) K were collected on two separate crystals on a Bruker Smart 1000 CCD using $Mo_{K\alpha}$ ($\lambda=0.71073$ Å) radiation and equipped with Oxford Instruments nitrogen gas (123 and 250 K structures) and helium gas (25 K structure) cryostreams. The first crystal was used in the 123 and 250 K full data collections and the variable-temperature unit-cell measurements by using the nitrogen gas cryostream. The second crystal was used in the 25 K full data collection and variable-temperature unit-cell measurements using the helium gas cryostream. Variable-temperature unit-cell determinations were carried out during the temperature-ramping profiles outlined above at a rate of 15 K h^{-1}. X-ray crystal data for $\mathbf{1}\cdot4CH_2Cl_2$ at 123 K were obtained following quench-cooling of the crystals from room temperature. The crystal data for $\mathbf{1}\cdot4CH_2Cl_2$ at 250 K were obtained following the heating of a crystal of $\mathbf{1}\cdot4CH_2Cl_2$ from 123 to 250 K at 15 K h^{-1}. X-ray crystal data for $\mathbf{1}\cdot4CH_2Cl_2$ at 25 K were obtained following the cooling of a crystal from 135 to 25 K at a rate of 15 K h^{-1}. Diffraction data for $\mathbf{1}\cdot CH_2Cl_2$ at 123 K was collected on a APEX X8 using $Mo_{K\alpha}$ ($\lambda=0.71073$ Å) radiation and equipped with an Oxford Instruments nitrogen gas cryostream. Empirical absorption corrections were applied to all data using SADABS.[22] The structures were solved with SHELXS-86 and refined with SHELXL-97[23] from data reduced with SAINT+ V.6.45.[24] All non-hydrogen atoms in the structures were refined anisotropically and hydrogen atoms were generated using the riding model.

Further details on the crystal structure investigation may be obtained from the Fachinformationszentrum Karlsruhe, 76344 Eggenstein-Leopoldshafen, Germany (fax: (+49) 7247-808-666; e-mail: crysdata@fiz-karlsruhe.de), on quoting the depository numbers CSD-292520, CSD-292521, CSD-292552 and CSD-607641.

Thermogravimetric analysis: The measurement was carried out on a TA instruments Hi-Res TGA 2950 Thermogravimetric Analyser. Decomposition analysis was performed over the temperature range 25–500°C at a heating rate of 1°C min^{-1}. The atmosphere was controlled with a dry dinitrogen supply (0.1 L min^{-1}).

Magnetic susceptibility measurements: Magnetic susceptibility data were collected using a Quantum Design MPMS 5 SQUID magnetometer under an applied field of 1 T. The samples were placed in a quartz tube and great care was taken to avoid any solvent loss and/or torquing of crystallites of these potentially anisotropic HS–HS iron(II) species. Care was also taken to allow long thermal equilibration times at each temperature point.

Mössbauer measurements: The spectra were measured using a conventional constant acceleration drive with a symmetrical sawtooth waveform. The source of ^{57}Co in rhodium was maintained at room temperature. Fresh crystalline samples were loaded into a piston type Perspex holder taking precautions, as much as possible, to avoid any solvent loss from the crystals that were damp with dichloromethane. The holder was placed in a cold-finger type cryostat in good thermal contact with a reservoir containing liquid nitrogen. The spectra were fitted to Lorentzian lines, with the matching lines of a doublet constrained to have the same intensity and line width.

Acknowledgements

C.J.K. and K.S.M. thank the Australian Research Council for funding by a Discovery Project grant. We thank M. B. Duriska for assistance with illustrations.

[1] K. S. Murray, C. J. Kepert, *Top. Curr. Chem.* **2004**, *233*, 195.
[2] J. A. Real, H. Bolvin, A. Bousseksou, A. Dworkin, O. Kahn, F. Varret, J. Zarembowitch, *J. Am. Chem. Soc.* **1992**, *114*, 4650.
[3] J. A. Real, A. B. Gaspar, V. Niel, M. C. Muñoz, *Coord. Chem. Rev.* **2003**, *236*, 121.
[4] A. B. Gaspar, M. C. Muñoz, J. A. Real, *J. Mater. Chem.* **2006**, *16*, 2522.
[5] B. A. Leita, B. Moubaraki, K. S. Murray, J. P. Smith, J. D. Cashion, *Chem. Commun.* **2004**, 156.
[6] K. Nakano, N. Suemura, S. Kawata, A. Fuyuhiro, T. Yagi, S. Nasu, S. Morimoto, S. Kaizaki, *Dalton Trans.* **2004**, 981.
[7] M. H. Klingele, B. Moubaraki, J. D. Cashion, K. S. Murray, S. Brooker, *Chem. Commun.* **2005**, 987.
[8] N. Ortega-Villar, A. L. Thompson, M. C. Muñoz, V. M. Ugalde-Sadívar, A. E. Goeta, R. Moreno-Esparza, J. A. Real, *Chem. Eur. J.* **2005**, *11*, 5721.
[9] C. Schneider, B. Moubaraki, K. S. Murray, S. M. Neville, unpublished data.
[10] P. J. Steel, C. Sumby, *Chem. Commun.* **2002**, 322.
[11] J. Pang, Y. Tao, S. Freiberg, X.-P. Yang, M. D'Iorio, S. Wang, *J. Mater. Chem.* **2002**, *12*, 206.
[12] K. Nakano, S. Kawata, K. Yoneda, A. Fuyuhiro, T. Yagi, S. Nasu, S. Morimoto, S. Kaizaki, *Chem. Commun.* **2004**, 2892.
[13] P. Gütlich, H. A. Goodwin, *Top. Curr. Chem.* **2004**, 233–235.
[14] P. Guionneau, C. Brigouleix, Y. Barrans, A. E. Goeta, J.-F. Létard, J. A. Howard, J. Gaultier, D. C. Chasseau, *C. R. Acad. Sci. Ser. IIc* **2001**, *4*, 161–171.
[15] P. Guionneau, M. Marchivie, G. Bravic, J.-F. Letard, D. Chasseau, *Top. Curr. Chem.* **2004**, *234*, 97.
[16] G. J. Halder, C. J. Kepert, B. Moubaraki, K. S. Murray, J. D. Cashion, *Science* **2002**, *298*, 1762.
[17] V. Niel, A. L. Thompson, M. C. Muñoz, A. Galet, A. S. E. Goeta, J. A. Real, *Angew. Chem.* **2003**, *115*, 3890; *Angew. Chem. Int. Ed.* **2003**, *42*, 3760.
[18] S. Bonhommeau, G. Molnár, A. Galet, A. Zwick, J. A. Real, J. J. McGarvey, A. Bousseksou, *Angew. Chem.* **2005**, *117*, 4137; *Angew. Chem. Int. Ed.* **2005**, *44*, 4069.
[19] E. Breuning, M. Ruben, J.-M. Lehn, F. Renz, Y. Garcia, V. Ksenofontov, P. Gütlich, E. Wegelius, K. Rissanen, *Angew. Chem.* **2000**, *112*, 2563; *Angew. Chem. Int. Ed.* **2000**, *39*, 2504.
[20] PLATON: A multipurpose crystallography tool, A. L. Spek, Utrecht University (The Netherlands), **2000**.
[21] S. Zein, S. A. Borshch, *J. Am. Chem. Soc.* **2005**, *127*, 16197.
[22] SADABS: Empirical adsorption correction program for area detector data, G. M. Sheldrick, University of Göttingen (Germany), **1996**.
[23] SHELXTL: Program for crystal structure solution and refinement, Bruker Analytical X-ray Instruments Inc., Madison, Wisconsin (USA), **1997**.
[24] SMART, SAINT and XPREP: Area detector and data integration and reduction software, Bruker Analytical X-ray Instruments Inc., Madison, Wisconsin (USA), **1995**.

Received: July 24, 2006
Published online: October 6, 2006

